Surface & Coatings Technology 301 (2016) 42–53

Contents lists available at ScienceDirect

Surface & Coatings Technology

journal homepage: www.elsevier.com/locate/surfcoat

Optimization of electrochemical step deposition for bioceramic hydroxyapatite coatings on CoCrMo implants

M. İbrahim Coşkun [a,b], İsmail H. Karahan [c], Yasin Yücel [d], Teresa D. Golden [a,*]

[a] Department of Chemistry, University of North Texas, 1155 Union Circle #305070, Denton, TX 76203, USA
[b] Department of Physics, Faculty of Arts and Sciences, Kilis 7 Aralık University, Kilis 79000, Turkey
[c] Department of Physics, Faculty of Arts and Sciences, Mustafa Kemal University, Hatay 31040, Turkey
[d] Department of Chemistry, Faculty of Arts and Sciences, Mustafa Kemal University, Hatay 31034, Turkey

ARTICLE INFO

Article history:
Received 14 October 2015
Revised 22 December 2015
Accepted in revised form 23 December 2015
Available online 29 December 2015

Keywords:
CoCrMo
Hydroxyapatite
Bioceramic
Central Composite Design
Response Surface Methodology
Electrodeposition

ABSTRACT

CoCrMo metallic implants were coated with a bioceramic hydroxyapatite layer using a modified step electrodeposition at room temperature. Response Surface Methodology (RSM) and Central Composite Design (CCD) were used to model and optimize the step deposition parameters, such as initial potential, scan rate and peak potential. Interactions between step deposition parameters and *in vitro* corrosion performance of the coatings were modeled by response surface plots. Predicted and experimental values were fitted with high accuracy. The effects of the step deposition parameters were evaluated within the limits of lowest applied potential (−0.03 to −1.17 V), scan rate (3.43–116.57 mV/s) and highest applied deposition potential (−1.08 to −1.92 V). A 5-level-3-factor experiment plan was used to optimize step deposition parameters. Optimum conditions for the modified step deposition parameters were determined as initial potential of −0.76 V, peak potential of −1.67 V and scan rate of 59.33 mV/s.

© 2015 Elsevier B.V. All rights reserved.

1. Introduction

Metallic biomaterials such as stainless steel, titanium alloys, and CoCrMo alloys are widely used in hip, knee and dental applications as a load-bearing implant material due to the superior mechanical properties and corrosion resistance [1]. Recently, CoCrMo alloys have been preferred as an alternative to other metallic implants due to higher strength and robust surface hardness, which improves their resistance to wear *in vivo* [2]. Additionally, CoCrMo alloys can be used at bearing surfaces of total joint arthroplasty (TJA) devices rather than Ti alloys [3].

However, metallic implants including CoCrMo alloys are not biocompatible materials and do not bond spontaneously to bone thus needing mechanical locking [4]. CoCrMo materials have poor biocompatibility and are encapsulated into the body by fibrous tissue which isolates them from the surrounding living organism [5]. Researchers are studying to modify implant surfaces on the nanometer scale consistent with *in vivo* physiological environment [6]. A bioceramic calcium phosphate (CaP) layer, such as hydroxyapatite, is widely used as a coating material to enhance biocompatibility of the metallic implants [7,8]. The porous nature of the hydroxyapatite layer improves osseointegration by providing more spaces for bone ingrowth, and the bond between biomaterial and bone becomes stronger [9]. According to recent studies, an improvement was observed at the bone contact level on hydroxyapatite coated CoCrMo implants compared to the uncoated ones [2].

Hydroxyapatite coatings on biometallic alloys have been formed by different methods such as plasma spray, sol–gel, magnetron sputtering, electrophoretic deposition, and electrodeposition [2,8]. Plasma spray is the only technique that has been clinically accepted, but this method has several disadvantages such as high operation temperature which effects the homogeneity of the coating [10], unpredictable phase changes of the coating during the deposition process, particle release and delamination [8]. Electrochemical deposition offers several advantages for fabrication of bioceramic coatings such as low fabrication temperature, control of composition, low cost of operation and ability to deposit on complex geometries [11,12]. Studies on hydroxyapatite coated implants prepared electrochemically are mainly focused on titanium, titanium alloys, and 316L stainless steel [13–16]. Limited number of studies have been reported on coating CoCrMo implants with hydroxyapatite by electrodeposition [17]. A literature survey revealed no reports on the optimization of step deposition parameters and studying their interactions using computational methods during the electrodeposition of hydroxyapatite on CoCrMo alloys. Due to these factors, improvement in the electrochemical deposition process to fabricate bioceramic coatings on metallic implants has great benefits for biomedical applications.

In vivo performance of a bioceramic coating is affected by properties such as phase content, crystal structure, surface morphology, and

* Corresponding author.
E-mail addresses: ibrahimcoskun27@gmail.com (M. İbrahim Coşkun), ihkarahan@gmail.com (İ.H. Karahan), yasinyucel@gmail.com (Y. Yücel), tgolden@unt.edu (T.D. Golden).

http://dx.doi.org/10.1016/j.surfcoat.2015.12.076
0257-8972/© 2015 Elsevier B.V. All rights reserved.

porosity. [13,14]. So, clinical performance of the hydroxyapatite coatings can be modified by a change in structure which results in different physical and chemical outcomes. Changing electrodeposition parameters such as applied potential, current density, pH, temperature and deposition time can change the structure of the coating [18]. Optimization of the electrodeposition parameters can allow for the fabrication of bioceramic coatings with desired properties. In this study, a novel coating process, modified step deposition was investigated to fabricate bioceramic hydroxyapatite coatings. Most of the traditional step deposition cycles include applying a constant potential with a following "cell off" time. We applied continuously increasing and decreasing potential cycles instead of constant potential steps.

To investigate the effects of several step deposition variables and determine the complete results of these effects on the coating performance, we performed a computational study using chemometric methods. Response Surface Methodology (RSM) is a useful chemometric approach to determine the interaction effects of experimental parameters and also to optimize main parameters with a minimum number of experiments [19]. RSM has been successfully applied in many different chemical processes [20–25]. Another modeling software, Central Composite Design (CCD), was used for further computational studies of RSM. In our study, *in vitro* corrosion tests on the coatings were chosen as the response for the RSM model. In a previous study, we successfully used RSM with CCD to optimize electrolyte solution parameters for hydroxyapatite coatings [26]. These optimized parameters were used in this study for preparation of the electrolyte solution.

In this research, RSM in combination with CCD was used to determine an optimized step deposition mode for electrodeposition of hydroxyapatite. The step deposition parameters (initial potential, scan rate and peak potential) were optimized by using a 5-level-3-factor CCD. The interactions between these parameters and the responses (*in vitro* corrosion performance of coatings) were analyzed systematically. Research results revealed that optimization of the step deposition parameters has a significant effect on the *in vitro* performance of the bioceramic coatings. Modifying deposition parameters to set and control properties of the bioceramic coatings are a promising method for designing biomaterials with desired properties.

2. Material and methods

2.1. Substrate preparation

Commercially provided CoCrMo (DIN EN ISO 22674) metallic implant materials were used as substrates. Composition of the CoCrMo biomaterial is: Co (58.3%), Cr (32%), Mo (6.5%), W (1.5%) and Si (1.0%). CoCrMo alloys were set into epoxy resin with an exposed circular surface area of 0.5 cm^2. Surface of the substrates were abraded mechanically with varying grit of SiC abrasive papers and alumina paste until a mirror like surface was achieved. After polishing, substrates were washed with deionized water and cleaned with an acetone:ethanol mixture ultrasonically. Prior to electrodeposition, the surface of the alloys were etched with 1 M HCl and then 10% HF acidic solutions for 10 s each, respectively, to remove oxide layers.

2.2. Fabrication of hydroxyapatite coatings

All solutions were prepared from reagent grade chemicals and ultrapure (18 MΩ) water (Aqua Solutions). A fresh electrolyte solution was used for each experiment. Composition of the solution determined from a previous optimization study, contained 0.05 M $Ca(NO_3)_2 \cdot 4H_2O$ and 0.04 M $NH_4H_2PO_4$ [26]. To suppress the negative effect of dihydrogen evolution and improve formation of a dense coating, 10 ml/L of 30% H_2O_2 was added to the solution [27]. Solution pH was increased to 4.7 using a dilute solution of ammonium hydroxide (NH_4OH), optimum pH was determined in a previous study [28,29]. Solutions were gently stirred during hydroxyapatite depositions to maintain uniformity.

All coating experiments were performed at room temperature (20 °C). An EG&G Princeton Applied Research (PAR) model 273A potentiostat/galvanostat was used for the hydroxyapatite coating experiments with a three electrode cell. Ag/AgCl electrode and a platinum plate were used as the reference and counter electrodes, respectively. All potential values for electrodeposition experiments are reported *versus* Ag/AgCl. During the electrodeposition experiments, temperature, electrolyte concentration, pH, deposition time, electrode area, *etc.* were kept constant to investigate only step deposition parameters. Electrodepositions of the hydroxyapatite coatings were performed with a modified step deposition method. Fig. 1 illustrates a typical cycle for the step deposition. Starting from an initial potential point (E_1) an increasing linear applied potential ramp in the cathodic region was performed until the peak potential point (E_2). Time from potential point E_1 to E_2 and E_2 to E_1 was varied in experiments due to varying scan speed times and varying potential points in the experiment plan. The plateau lasted 1 s in each step cycle. Tables 1 and 2 list these experimental parameters for each deposit. Each electrodeposition experiment was performed for 90 min with continuous step deposition cycles. At the beginning of the electrodeposition, current values were about 4 mA/cm^2 but dropped to 40 μA/cm^2 levels after 1 h. This significant current decrease was caused by the formation of the non-conducting bioceramic layer which reduces current flow through the working electrode. These low current densities indicated that the substrate surface was well covered with a hydroxyapatite layer. After the electrodeposition process, coated samples were washed with deionized water and dried in air. Formation of the hydroxyapatite layer on CoCrMo implant surface can be explained by the following reactions [14,15,30,31]:

$$2H_2O + 2e^- \rightarrow H_2 + 2OH^- \quad (1)$$

$$H_2O_2 + 2e^- \rightarrow 2OH^- \quad (2)$$

$$2HPO_4^{2-} + 2e^- \rightarrow H_2 + 2PO_4^{3-} \quad (3)$$

$$HPO_4^{2-} + OH^- \rightarrow PO_4^{3-} + H_2O \quad (4)$$

$$10Ca^{2+} + 6PO_4^{3-} + 2OH^- \rightarrow Ca_{10}(PO_4)_6(OH)_2 \quad (5)$$

Reduction of the H_2O_2 and H_2O in reactions (1) and (2) leads to the formation of OH^- ions and causes an increase in the local pH of the electrolyte at the cathode interface. Since the pH is highest next to the electrode surface, heterogeneous deposition is favored over homogeneous precipitation in the bulk. In addition, a reduction reaction (3) or reaction with the generated base (4) can produce PO_4^{3-} ions. Anions in solution

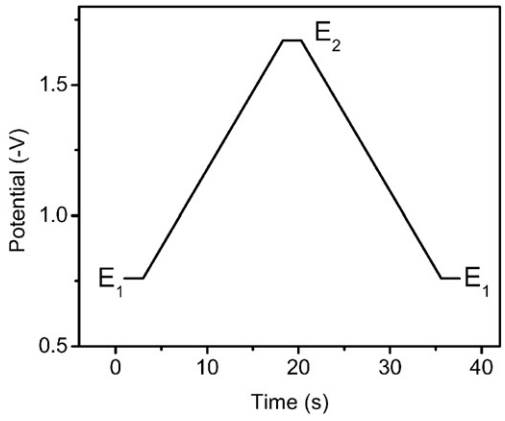

Fig. 1. Representation of a cycle of the modified step electrodeposition.

Table 1
Independent variables and levels used for response surface design.

Independent variables	Symbols	Levels				
		−1.414	−1	0	1	1.414
E_1 (V)	A	−0.03	−0.20	−0.60	−1.00	−1.17
E_2 (V)	B	−1.08	−1.20	−1.50	−1.80	−1.92
Scan rate (mV/s)	C	3.43	20	60	100	116.57

Table 2
Central Composite Design of the depositions with coded and actual values of variables.

Run	Coded independent variable levels			Actual values of variables		
	A	B	C	A	B	C
	E_1 (V)	E_2 (V)	Scan rate (mV/s)	E_1 (V)	E_2 (V)	Scan rate (mV/s)
1	1	1	−1	−1.0	−1.8	20
2	1	−1	1	−1.0	−1.2	100
3	−1	1	1	−0.2	−1.8	100
4	−1	−1	−1	−0.2	−1.2	20
5	−1.414	0	0	−0.03	−1.5	60
6	1.414	0	0	−1.17	−1.5	60
7	0	−1.414	0	−0.6	−1.08	60
8	0	1.414	0	−0.6	−1.92	60
9	0	0	−1.414	−0.6	−1.5	3.43
10	0	0	1.414	−0.6	−1.5	116.57
11	0	0	0	−0.6	−1.5	60
12	0	0	0	−0.6	−1.5	60
13	0	0	0	−0.6	−1.5	60
14	0	0	0	−0.6	−1.5	60
15	0	0	0	−0.6	−1.5	60

combine with the calcium to obtain the final product, the precipitation of the hydroxyapatite on the CoCrMo surface (5).

2.3. Experimental design

2.3.1. Model for experiments

CCD is an experimental design which is combined with RSM studies to build a second order model to explain the responses. 15 sets of electrodeposition experiments with varying step deposition parameters including: initial potential (E_1), peak potential (E_2) and scan rate were designed by CCD according to manually determined ranges. Preliminary experiments determined ranges of the step deposition parameters for electrodeposition of the hydroxyapatite. The variable parameters with applied ranges and level codes are listed in Table 1. The experimental plan applied for electrodepositions with actual and coded values of the variables are given in Table 2.

To optimize the step deposition parameters, three responses were chosen from the electrochemical corrosion analyses on the resulting coatings. Corrosion potential (E_{corr}) values from the potentiodynamic polarization analysis, open circuit potential (OCP) values from the immersion tests, and impedance values at low frequency region (0.1 Hz) from the electrochemical impedance spectroscopy (EIS) analysis were taken as responses (Y) for the models. OCP and E_{corr} values are an important indicator of barrier properties and breakdown potential of the coatings in simulated body fluid (SBF) [32]. More anodic OCP and E_{corr} values indicate a more chemically stable nature of the coatings and improvement of the anti-corrosion performance in SBF [33,34]. Also, impedance values at low frequency region are an important parameter to compare *in vitro* corrosion performance of the coatings [35]. All 3 responses were modeled with RSM.

2.3.2. Formulation of the models

Regression analyses were applied on the experimental results using software Design Expert 7.0.0 (Stat-Ease, Inc., Minneapolis, USA). The effect of step deposition parameters (E_1, E_2 and scan rate) was calculated both mutually and individually by the Design Expert. The E_{corr}, OCP and impedance values (Y values) of hydroxyapatite coatings were used to form three quadratic polynomial equations (Eq. (6)). The polynomial equations were solved separately according to three responses to determine the relationship and interactions between the responses and the independent variables.

$$Y = b_0 + \sum_{i=1}^{3} b_i X_i + \sum_{i=1}^{3} b_{ii} X_i^2 + \sum \sum_{i<j}^{3} b_{ij} X_i X_j \quad (6)$$

In Eq. (6), Y is the response value and b_0 indicates the offset term. X_i is the ith independent variable and X_j is the jth independent variable. Independent variables X_1, X_2 and X_3 are: initial potential, peak potential, and scan speed respectively. b_i is the linear effect, b_{ii} is the squared effect of the variables. b_{ij} is the interaction effect between the variables X_i and X_j.

2.3.3. Determining accuracy of the models

The statistical significance of the models was controlled by an F-test according to F-values. Regression analysis was performed for the responses in order to estimate the effect of combined and independent variable parameters on each response. Linear, quadratic and cubic models were tested to find the best fitting model with responses. Second order polynomial equations were used to determine regression coefficients. The effect of each term in the models was calculated by analysis of variance (ANOVA). The fit of the models was determined

Table 3
Central Composite Design of factors with the experimental and the predicted values.

Run	E_{corr} (V)		OCP (V)		Impedance (kΩ)	
	Experimental	Predicted	Experimental	Predicted	Experimental	Predicted
1	−0.250	−0.263	−0.232	−0.232	148	143
2	−0.313	−0.326	−0.276	−0.276	110	105
3	−0.595	−0.608	−0.521	−0.521	14	9
4	−0.246	−0.259	−0.211	−0.211	121	116
5	−0.210	−0.197	−0.270	−0.270	110	115
6	−0.268	−0.255	−0.239	−0.239	113	118
7	−0.554	−0.541	−0.380	−0.380	62	67
8	−0.340	−0.327	−0.252	−0.252	128	133
9	−0.360	−0.347	−0.312	−0.312	30	35
10	−0.273	−0.260	−0.300	−0.300	107	112
11	−0.233	−0.236	−0.275	−0.255	96	106
12	−0.218	−0.236	−0.224	−0.255	120	106
13	−0.212	−0.236	−0.273	−0.255	111	106
14	−0.243	−0.236	−0.283	−0.255	115	106
15	−0.249	−0.236	−0.219	−0.255	97	106

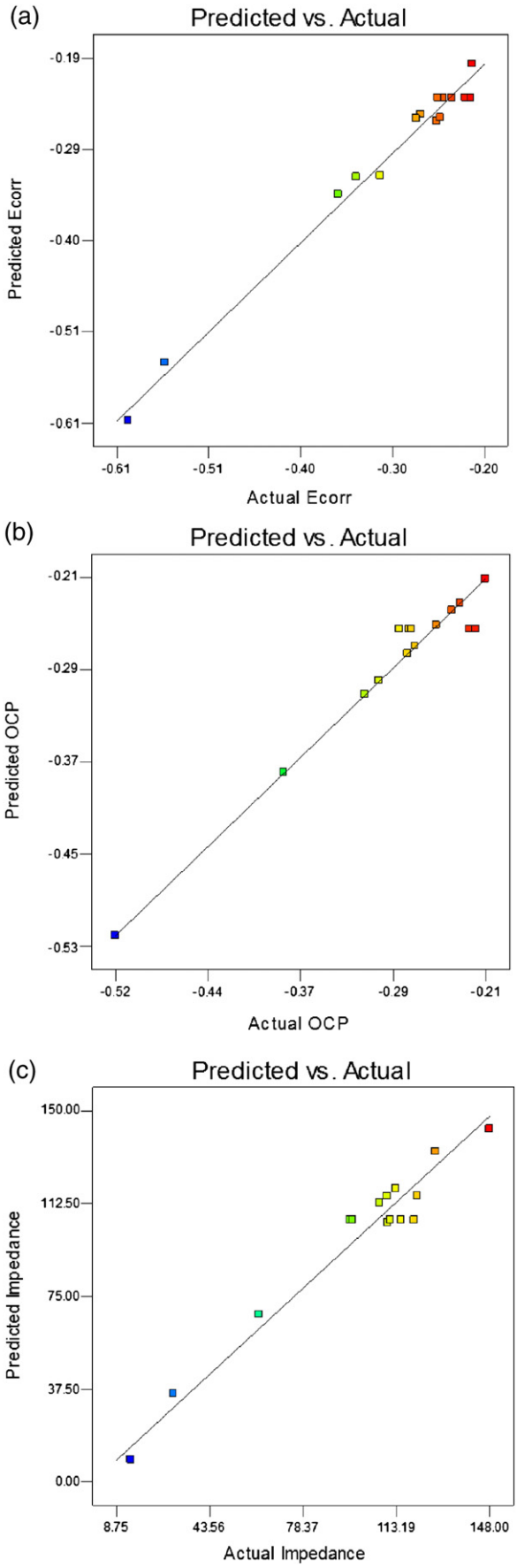

Fig. 2. Actual (squares) and predicted (line) values of the RSM models for (a) E_{corr}; (b) OCP and (c) impedance.

Table 4
Second order polynomial equations and regression coefficients of the response variables (A: E_1; B: E_2; C: scan rate).

Responses	Second order polynomial equations
Ecorr (V)	$y = -0.24 - 0.021A + 0.076B + 0.031C + 0.13AB + 0.15\,AC - 0.090BC + 0.005A^2 - 0.099B^2 - 0.034C^2$
OCP (V)	$y = -0.25 + 0.011A + 0.045B + 0.0042C + 0.093AB + 0.11\,AC - 0.045BC + 0.00037A^2 - 0.030B^2 - 0.025C^2$
Impedance (kΩ)	$y = +105.62 + 1.10A + 23.33B + 27.22C + 63.42AB + 40.53\,AC - 29.60BC + 5.64A^2 - 2.58B^2 - 15.83C^2$

Table 5
Analysis of variance (ANOVA) of the fitted quadratic polynomial model for $E_{corr.}$

Source	Sum of squares	Degree of freedom	Mean square	F-value	P-value (Prob > F)
Model	0.19	9	0.022	38.60	0.0004[a]
A (E_1)	1.682E-003	1	1.682E-003	3.01	0.1431[b]
B (E_2)	0.023	1	0.023	41.02	0.0014[a]
C (Scan rate)	3.785E-003	1	3.785E-003	6.78	0.0480[a]
AB	0.036	1	0.036	64.10	0.0005[a]
AC	0.043	1	0.043	77.59	0.0003[a]
BC	0.016	1	0.016	29.03	0.0030[a]
A^2	1.936E-004	1	1.936E-004	0.35	0.5815[b]
B^2	0.076	1	0.076	135.42	<0.0001[a]
C^2	8.782E-003	1	8.782E-003	15.73	0.0107[a]
Residual	2.791E-003	5	5.582E-004		
Lack of fit	1.789E-003	1	1.789E-003	7.14	0.0557[b]
Pure error	1.002E-003	4	2.505E-004		
Cor total	0.20	14			
$R^2 = 0.9858$					

[a] Significant at "Prob > F" less than 0.05.
[b] Insignificant at "Prob > F" more than 0.05.

according to R^2 values. Response surface with contour plots was used to determine optimum parameters for the step deposition.

2.4. Characterization of hydroxyapatite coatings

In vitro analyses: OCP, potentiodynamic polarization and EIS measurements for hydroxyapatite coated implants were performed with an electrochemical analyzer (PARSTAT 4000, AMETEK) equipped with Versa Studio software. A simulated body fluid (SBF) at 37 ± 1 °C prepared according to the Ringer's solution recipe (Cold Spring Harbor Protocols) was used in the electrochemical analyses. Chemical composition of the SBF is 7.2 g NaCl, 0.37 g KCl, 0.17 g $CaCl_2$ for a 1000 mL solution. Tris(hydroxymethyl)aminomethane (TRIS) was used to buffer the pH of SBF to 7.4 ± 0.1. OCP was recorded as a function of time until the potential stabilized. EIS analyses were performed in the frequency range from 10^{-2} to 10^5 Hz. A 10 mV perturbation signal at OCP was applied. ZView (ver. 3.4) was used to further analyze the EIS results. Equivalent circuit elements were calculated by ZView according to the fitted EIS data. Potentiodynamic polarization measurements were carried out with a scan rate of 1 mV/s from −250 to +250 mV *versus* OCP. All potential values for *in vitro* analyses were with respect to the Ag/AgCl reference electrode. Surface morphology of the coatings was examined with a scanning electron microscope (SEM) FEI Quanta 200 ESEM, equipped with a Schottky field emission gun (FEG). After SEM analyses, the hydroxyapatite layer was scraped from the substrate surface for FTIR analyses. A FTIR spectrometer (PerkinElmer Spectrum One) was used to examine composition and chemical structure of the hydroxyapatite. FTIR spectra were recorded at a range between 450 and 4000 cm^{-1} and 16 scans were collected at 4 cm^{-1} resolution per sample.

Table 6
Analysis of variance (ANOVA) of the fitted quadratic polynomial model for OCP.

Source	Sum of squares	Degree of freedom	Mean square	F-value	P-value (Prob > F)
Model	0.082	9	9.114E-003	12.10	0.0067[a]
A (E_1)	4.805E-004	1	4.805E-004	0.64	0.4607[b]
B (E_2)	8.192E-003	1	8.192E-003	10.88	0.0215[a]
C (Scan rate)	7.200E-005	1	7.200E-005	0.096	0.7696[b]
AB	0.017	1	0.017	22.84	0.0050[a]
AC	0.025	1	0.025	33.16	0.0022[a]
BC	4.057E-003	1	4.057E-003	5.39	0.0680[b]
A^2	1.058E-006	1	1.058E-006	1.405E-003	0.9716[b]
B^2	7.120E-003	1	7.120E-003	9.45	0.0276[a]
C^2	4.969E-003	1	4.969E-003	6.60	0.0501[b]
Residual	3.766E-003	5	7.532E-004		
Lack of fit	1.070E-006	1	1.070E-006	1.137E-003	0.9747[b]
Pure error	3.765E-003	4	9.412E-004		
Cor total	0.086	14			
$R^2 = 0.9561$					

[a] Significant at "Prob > F" less than 0.05.
[b] Insignificant at "Prob > F" more than 0.05.

3. Results and discussion

3.1. Optimization of electrodeposition parameters

Optimization of the step deposition parameters for high corrosion resistant hydroxyapatite coatings was completed with RSM. Table 3 shows the experimental and the predicted values for the responses according to E_{corr}, OCP and impedance models. The experimental values of the E_{corr} varied from −0.595 to −0.212 V, values of the OCP varied from −0.521 to −0.211 V and values of the impedance at low frequency region (0.1 Hz) varied from 14 to 148 kΩ. The relationship between predicted and experimental response values is shown in Fig. 2. The experimental response values correctly matched the predicted data. The R^2 values for E_{corr}, OCP and impedance models are 0.9858, 0.9561, and 0.9572, respectively. The effect of each deposition parameter and the interaction with other parameters were investigated using Design Expert. The formulations of the models for the 3 responses are given in Table 4 by the second order polynomial equations.

The ANOVA is presented to show statistical significance of the formulations for the responses of the quadratic model. The significance of the model terms is explained by probability (P) > F values. For probability (P) > F values which are equal or less then 0.05, model terms are accepted as significant. If probability values are greater than 0.05, the model terms cannot be accepted as significant. Calculation results of the ANOVA study are given in Tables 5–7.

Table 7
Analysis of variance (ANOVA) of the fitted quadratic polynomial model for impedance.

Source	Sum of squares	Degree of freedom	Mean square	F-value	P-value (Prob > F)
Model	17,612.27	9	1956.92	12.42	0.0063[a]
A (E_1)	4.81	1	4.81	0.030	0.8682[b]
B (E_2)	2178.00	1	2178.00	13.82	0.0137[a]
C (Scan rate)	2964.50	1	2964.50	18.81	0.0074[a]
AB	8045.11	1	8045.11	51.05	0.0008[a]
AC	3286.10	1	3286.10	20.85	0.0060[a]
BC	1752.79	1	1752.79	11.12	0.0207[a]
A^2	245.61	1	245.61	1.56	0.2672[b]
B^2	51.45	1	51.45	0.33	0.5925[b]
C^2	1933.70	1	1933.70	12.27	0.0172[a]
Residual	788.02	5	157.60		
Lack of fit	321.22	1	321.22	2.75	0.1724[b]
Pure error	466.80	4	116.70		
Cor total	18,400.29	14			
$R^2 = 0.9572$					

[a] Significant at "Prob > F" less than 0.05.
[b] Insignificant at "Prob > F" more than 0.05.

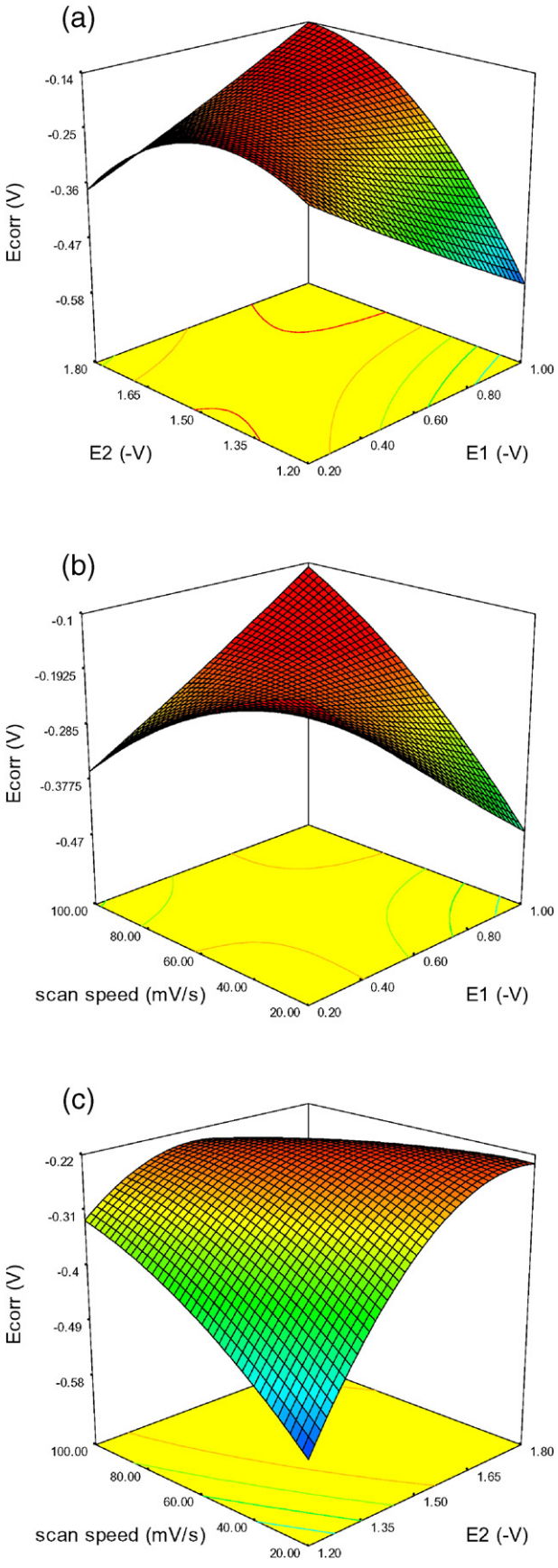

Fig. 3. Response surface plots of the E_{corr} predicted from the quadratic model. The effect of (a) E_1, E_2; (b) E_1, scan rate; (c) E_2, scan rate.

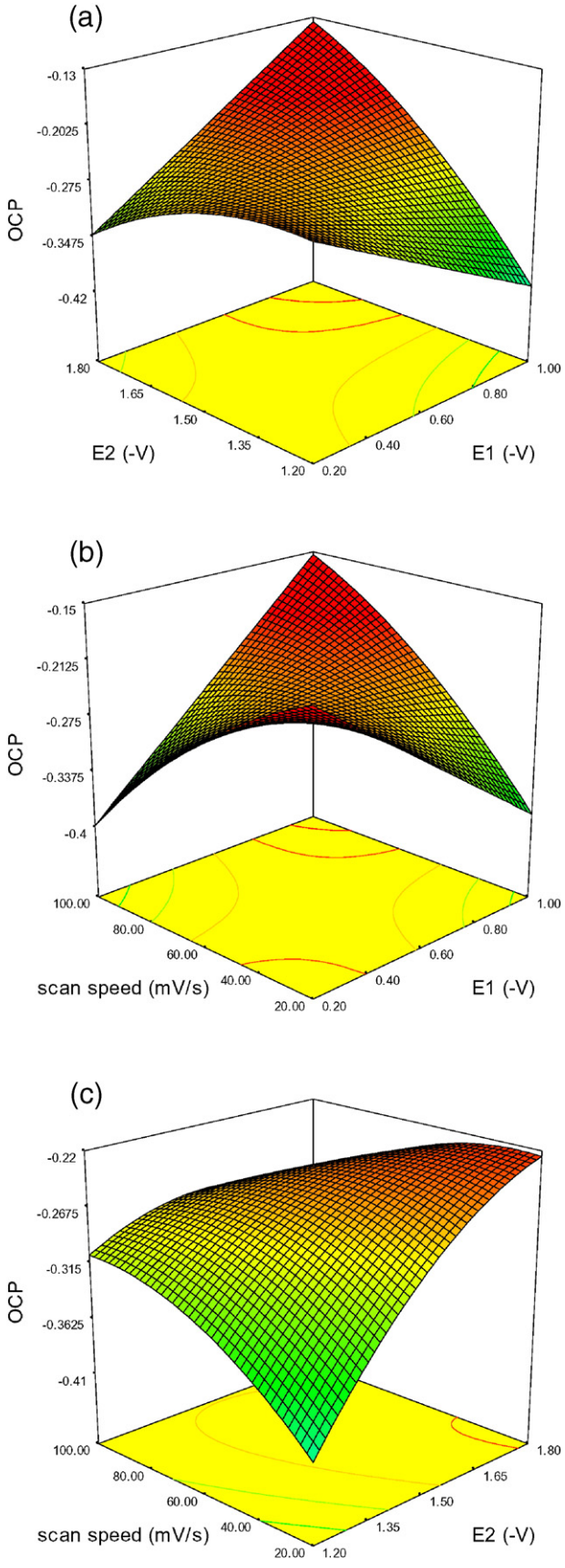

Fig. 4. Response surface plots of the OCP predicted from the quadratic model. The effect of (a) E_1, E_2; (b) E_1, scan rate; (c) E_2, scan rate.

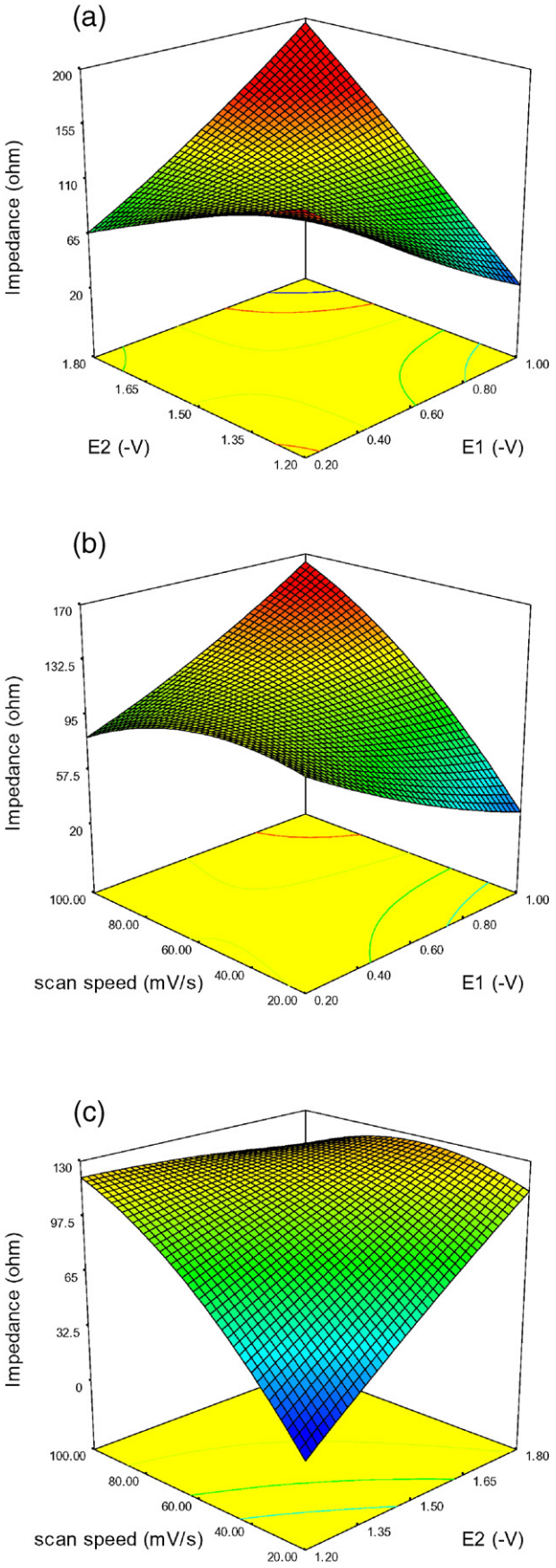

Fig. 5. Response surface plots of the impedance predicted from the quadratic model. The effect of (a) E_1, E_2; (b) E_1, scan rate; (c) E_2, scan rate.

The computed F-values for E_{corr}, OCP and impedance models are 38.60, 12.10 and 12.42, respectively, indicating significance of the models. Furthermore, the error values for E_{corr}, OCP and impedance are low, 0.0004, 0.0067, and 0.0063, respectively, which indicates reproducibility of the data and high coefficients of determination. According to the R^2 and F-values, the E_{corr} model is the best model among the three. The coefficients of determination indicate that there are significant correlations between the step deposition parameters: initial potential, peak potential, and scan rate. The lack of fits (F-values: 7.14, 0.00114 and 2.75) for regression of the equations (Table 4) are not significant. Non-significant lacks of fits indicate models are reliable. ANOVA results confirm the model equations are adequate for predicting the corrosion performance of coatings.

The significance of the model terms was determined by P-values. According to E_{corr} model (Table 5), B (peak potential), B^2, AB, AC, BC, C (scan rate), and C^2 are the most significant parameters. Variable A (initial potential) and A^2 have less effects on the corrosion performance of the hydroxyapatite coatings.

3.2. Interaction between independent variables of hydroxyapatite coatings

RSM was used to optimize and determine the interaction between the step deposition parameters and the quality of the hydroxyapatite coatings. The interaction between step deposition parameters and *in vitro* corrosion results (E_{corr}, OCP and impedance) was investigated by response surface plots. The response surface plots for the interaction effects of initial potential (E_1), peak potential (E_2), scan rate are shown in Figs. 3–5.

Response surface plots according to the E_{corr} model are given in Fig. 3. Interaction between E_1 and E_2 for the E_{corr} values is shown in Fig. 3a. For lower (more negative) E_1 values, an increase in the positive direction was observed in E_{corr} values with the decreasing of E_2. For higher (more positive) E_1 values, higher E_{corr} values were observed with higher E_2 values. The most negative E_{corr} value was observed for the lowest E_1 (−1.0 V) and the highest E_2 (−1.2 V) values. More positive E_{corr} values were observed when E_2–E_1 difference is larger than 0.8 V. The change of the E_{corr} with E_1 and E_2 values indicates that there must be a large enough gap between initial and peak potential values to deposit a coating with good corrosion performance. This behavior can be attributed to a period between depositions and relaxation time during the step deposition cycles. Applying lower E_1 with higher E_2 values decreases the period needed for deposition and relax time.

Interaction between E_1 and scan rate for E_{corr} values is given in Fig. 3b. The plot indicates lower scan rate values with lower E_1 or higher scan rate values with higher E_1 values has a negative effect on the E_{corr}. Applying low E_1 (−1.0 V) or high scan rate values decreases deposition time in a step deposition cycle. More positive E_{corr} values were observed for scan rate values about 60 mV/s and E_1 values at −0.7, −0.8 V levels which were confirmed with the model results (Section 3.3).

In Fig. 3c, surface plot of the relationship between E_2 and scan rate is displayed. According to the plot, a change in the E_2 values from −1.2 to −1.8 V results in more positive E_{corr} values in the low scan rate region. At scan rate values about 50–60 mV/s and E_2 values around −1.6 and −1.8 V, more positive E_{corr} values were observed. E_{corr} values shifted in the negative direction at E_2 values around −1.4 and −1.2 V and lower scan rate values. It is suggested that for a modified step deposition a more cathodic peak potential must be applied to fabricate protective bioceramic coatings.

Plots of the other responses, OCP and impedance are quite similar with plots of E_{corr} as shown in Figs. 4 and 5. Since all responses are indicative of the *in vitro* corrosion performance of the coatings, similar interactions are expected. According to the plots of OCP, for E_1–E_2 interaction (Fig. 4a) more positive OCP values were observed at E_1 values from −0.8 to −1.0 V with E_2 values from −1.65 to −1.8 V. According to E_1-scan rate interaction, E_1 values from −0.6 to −1.0 V with scan rate values around 60–80 mV/s resulted in higher OCP values (Fig. 4b). For E_2-scan rate interaction at lower E_2 values scan rate values higher than 50–60 mV/s caused a decrease in OCP values (Fig. 4c).

According to the response plots of impedance, higher impedance values were observed at E_1 values from −0.8 to −1.0 V with E_2 values at −1.7 V levels for E_1–E_2 interaction (Fig. 5a). Similarly, E_1 values around −0.8 to −1.0 V with scan rate values around 60–100 mV/s resulting in higher impedance values (Fig. 5b). E_2-scan rate plots (Fig. 5c) indicated an increase in E_2 (>−1.65 V) and decrease in scan rate values (<60 mV/s), respectively, and has a negative effect on the impedance values for the coatings.

Overall, as a result of the interaction studies, to fabricate hydroxyapatite coatings with high corrosion performance, an initial potential (E_1) at around −0.8 V, a peak potential (E_2) at around −1.65 V, and a scan rate at 60 mV/s must be applied for the modified step deposition.

3.3. Validation of the model

Model equations were solved to calculate optimum step deposition parameters E_1, E_2 and scan rate. It is expected to get similar optimized values from models designed according to corrosion performances (E_{corr}, OCP and impedance) of the coatings. According to E_{corr}, OCP and impedance models optimized values are; for E_1: −0.76, −0.83 and −0.86 V; for E_2: −1.67, −1.66, and −1.65 V; for scan rate: 59.33,

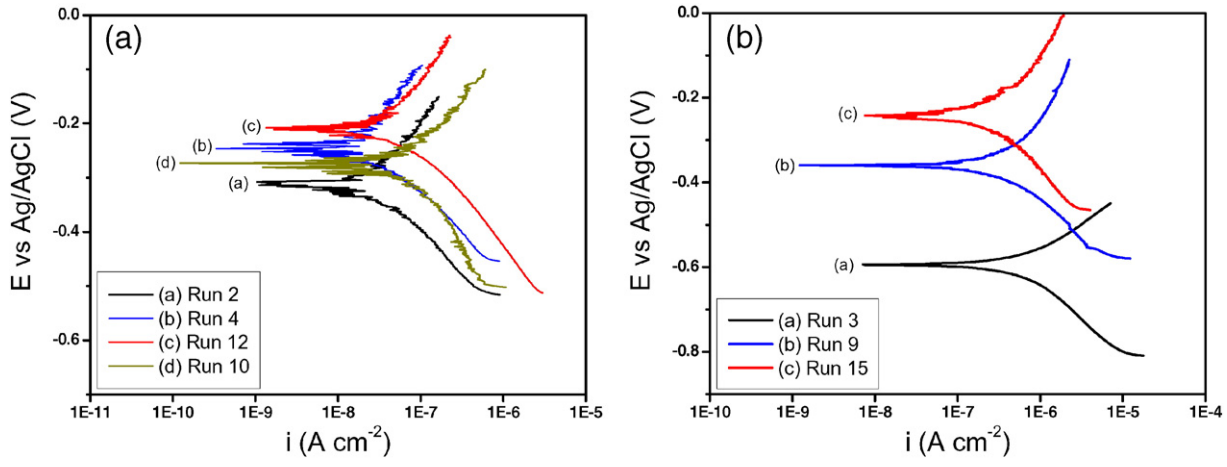

Fig. 6. Potentiodynamic polarization curves of runs (a) 2, 4, 10 and 12 and (b) 3, 9 and 15.

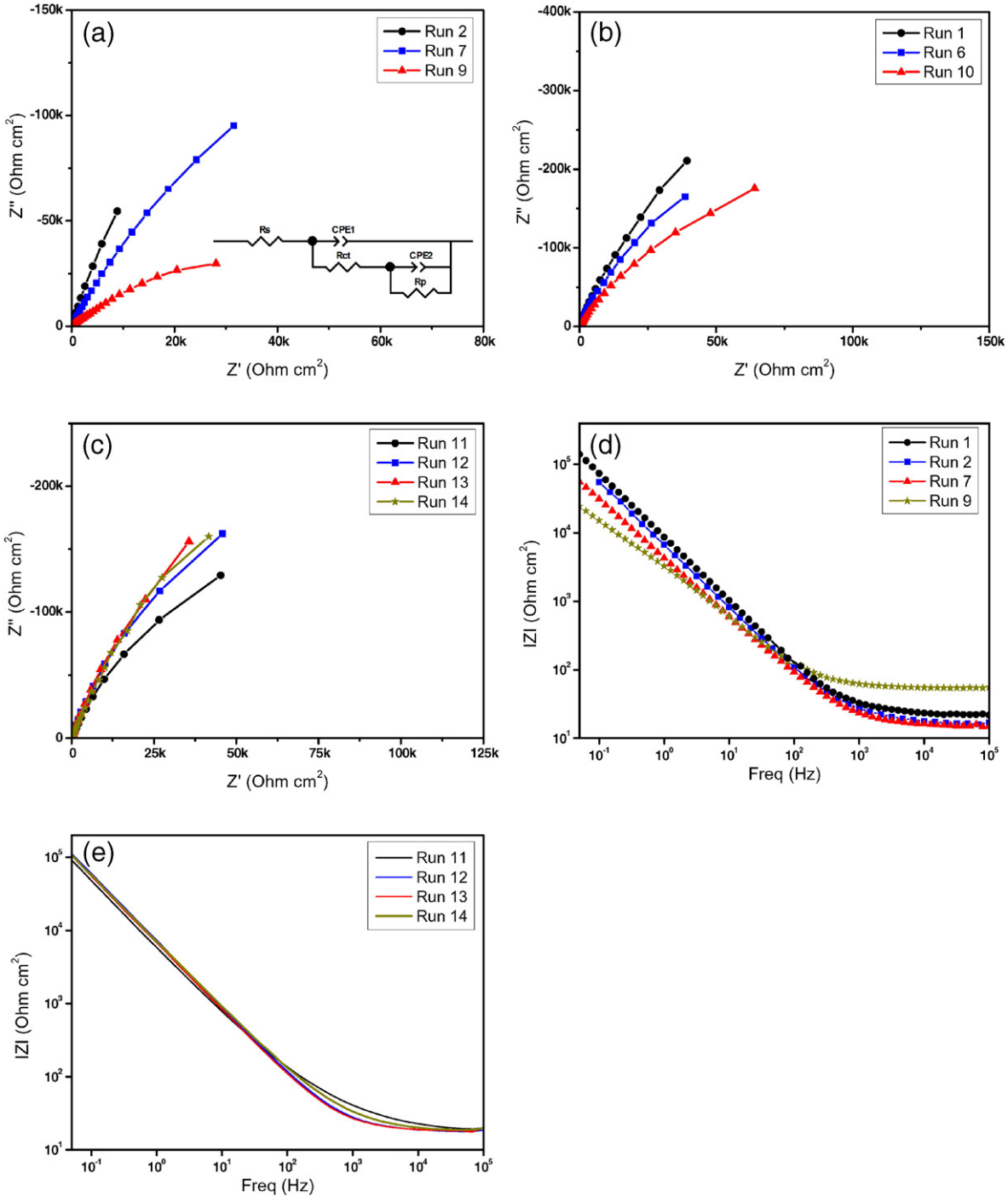

Fig. 7. EIS analysis results: (a) Nyquist plots of runs 2, 7 and 9 (b) Nyquist plots of runs 1, 6 and 10 (c) Nyquist plots of runs 11–14 (d) Bode plots of runs 1, 2, 7 and 9 and (e) Bode plots of runs 11–14.

60.41 and 69.51 mV/s respectively. The optimized values are very similar in all 3 models, especially for the significant parameters such as E_2 and scan rate. According to R^2 and F-values from ANOVA analysis, the E_{corr} model was the most applicable of the 3 models. Validity of the E_{corr} model was confirmed by verification experiments. Accuracy of the model was also checked by a sample (run 16) which was fabricated under the optimized conditions. Corrosion performance, FTIR and SEM analyzes confirmed the quality of fabricated coatings at optimized parameters.

3.4. Electrochemical analyses

3.4.1. Open circuit potential (OCP) measurements

Coatings were immersed in SBF about an hour before EIS and potentiodynamic polarization tests to stabilize the potential and record the OCP values. OCP values of all samples are given in Table 3. OCP values of the coatings in SBF reached a stable value rapidly indicating the passive nature of the coatings. Probably an oxide film began to grow after immersion in SBF which results in a relatively stable response [6].

Table 8
ZView analyses of the equivalent circuit elements.

Run	R_s (Ω cm^2)	R_{ct} (Ω cm^2)	C_{pe1}	C_{pe1-n}	C_{pe2}	C_{pe2-n}	R_p (Ω cm^2)
1	22.01	18.58	8.6803E-6	0.9334	1.2162E-5	0.9216	3.5781E6
2	16.4	23.27	1.2111E-5	0.9163	1.5782E-5	0.9044	1.749E6
3	94.14	4701	2.8391E-5	0.4491	1.0447E-4	0.5376	2.845E4
4	17.32	95.07	1.8344E-5	0.9116	7.7342E-6	0.8955	2.1706E6
5	15.58	85.28	1.7308E-5	0.9029	9.6398E-6	0.8860	1.2941E6
6	17.61	31.72	1.2425E-5	0.9304	1.4923E-5	0.9197	1.7184E6
7	15.25	49.88	3.2786E-5	0.8617	1.5288E-5	0.8413	1.4129E6
8	22.32	30.1	9.636E-6	0.9191	1.4314E-5	0.9126	4.844E6
9	47.68	8.86	4.2987E-5	0.5395	4.4454E-5	0.8243	2.74E5
10	18.08	172.2	1.9546E-5	0.8884	8.9189E-6	0.8852	1.2081E6
11	20.07	81.0	1.3791E-5	0.8690	1.854E-5	0.8890	1.3247E6
12	18.06	50.26	1.5657E-5	0.9180	9.8586E-6	0.9003	1.4478E6
13	18.39	56.79	1.7969E-5	0.9170	9.4609E-6	0.8996	1.707E6
14	18.99	67.91	1.433E-5	0.8979	1.238E-5	0.8890	1.8689E6
15	18.71	604.1	2.8925E-5	0.9287	3.7648E-6	0.9514	1.2889E6
16	19.55	66.07	2.0367E-5	0.8769	2.0367E-5	0.8768	7.5343E6

More positive OCP values indicate more chemical stability for the coatings and improvement in the corrosion performance [34,36]. As seen in Table 3, runs 1, 4, 6, 8, and 11–15 have more positive OCP values, about −0.25 V. Runs 3, 7 and 9 have more negative OCP values: −0.52, −0.38, and −0.312 V respectively. According to the OCP results, runs 3, 7, and 9 did not present a stable nature compared to other samples.

3.4.2. Potentiodynamic polarization measurements

The E_{corr} values presented in Table 3 were obtained from potentiodynamic polarization tests and plots of selected samples are shown in Fig. 6. E_{corr} values from Tafel plots are indicative values for *in vitro* corrosion behavior of the coatings [32]. A positive shift in E_{corr} values indicates a more passive nature of the hydroxyapatite coatings [11] that leads to a better corrosion resistance for the CoCrMo alloy [32]. As seen in Fig. 6a and Table 3 runs 2, 4, and 10–15 have more positive E_{corr} values compared to runs 3, 7, 8, and 9. Deposition parameters of runs 11–15 were the same (E_1: −0.6 V, E_2: −1.5 V, scan rate: 60 mV/s). This part of the experimental plan is to check robustness of the experimental design. Similar experimental results are expected from these samples. In addition, the deposition parameters for these samples are the most similar parameters to the optimized parameters (E_1: −0.76 V, E_2: −1.67 V, scan rate: 59.33 mV/s) determined by the E_{corr} model. Therefore, high corrosion performance is expected from these samples. As listed in Table 3, E_{corr} values of these samples were similar (around −0.25 V) indicating high *in vitro* corrosion performance in SBF.

As explained in Section 3.2, the model study indicated there must be a large enough potential difference in the modified step deposition between E_1 and E_2 to achieve good barrier properties. According to the experimental plan, runs 1, 4, and 10–15 have a potential range of about 1.0 V. E_{corr} values of these samples were more positive compared to other samples confirming the model study. For the significant parameters: E_2 and scan rate, run 6 has similar deposition parameters (E_2: −1.5 V, scan rate: 60 mV/s) with the optimized parameters (E_2: −1.67 V, scan rate: 59.33 mV/s). Corrosion resistance of this sample is relatively high according to Table 3, as expected.

Experimental E_{corr} values of runs 3, 7, and 9 are −0.595, −0.554, and −0.360 V, respectively, which indicates poorer corrosion resistance. OCP values of these samples were also more negative compared to other coatings. All deposition parameters of run 3 are far away from optimum parameters and probably caused this poor corrosion performance. Run 7 has a peak potential value of −1.08 V, which is the lowest among all other coatings. It is suggested that extremely low E_2 values of this sample prevented good hydroxyapatite formation. Run 9 has a scan rate value of 3.43 mV/s, which is the lowest in the experiment plan. This extremely low scan rate is probably the main reason for the relatively low E_{corr} value.

3.4.3. Electrochemical impedance spectroscopy (EIS) measurements

For Nyquist plots, a bigger capacitive loop diameter corresponds to a higher corrosion resistance [37]. Also, low frequency impedance (Z) values from Bode plots can be used to compare corrosion performance of the coatings [35]. As seen in Fig. 7a–c, runs 1, 6, and 10–15 have bigger capacitive loop diameters compared to runs 2, 7, and 9. Low frequency impedance values of these samples (Fig. 7d) were also comparably higher. According to the EIS graphs, runs 2, 7, and 9 have relatively low corrosion performance compared to other samples, as observed in the OCP and Tafel results.

EIS results were modeled by ZView software to achieve more information about corrosion behavior in SBF. An equivalent electrical circuit was used to model the interaction between the sample and SBF, as shown in Fig. 7a (inset). In the equivalent electrical circuit, R_S displays resistance of the SBF solution. R_{ct} equals the charge transfer resistance, related to resistance of the porous coating surface. R_p represents polarization resistance or resistance of the coating. R_p is inversely proportional to the corrosion current density, i_{corr}, and the major element representing corrosion resistance of the hydroxyapatite layer in SBF. Constant phase element (C_{pe1}) represents the coating capacitance, capacitance of the outer porous layer. C_{pe2} is the double layer capacitance and represents the interface between solution and sample [11,38]. Calculated circuit elements by ZView software are presented in Table 8 with Rp values fitted at lowest frequency of 0.01 Hz.

R_s values of the samples were mostly around 20 Ω as expected from a conductive solution. R_{ct} values of the samples mostly varied from 10^1 to 10^2 Ω cm^2, understandable for a porous coating surface. According to ZView calculations corrosion performance of runs 3 and 9 is poor compared the other samples in experimental plan. R_p values of these samples are at 10^4–10^5 Ω cm^2 levels while other samples are at 10^6 Ω cm^2 levels. Run 16, sample fabricated at optimized parameters has the highest R_p value, 7.53 10^6 Ω cm^2.

Deposition parameters of the runs 11–15 were the same. As seen in Fig. 7c and e, Nyquist and Bode plots of these samples are very similar, even overlapping as expected. Also, R_p values of these samples are similar, and varied between 1 and 2 10^6 Ω cm^2. EIS and ZView results are well matched with the RSM model predictions and polarization analyses. Most of the coatings have an R_p value around 10^6 Ω cm^2 indicating a protective barrier nature in SBF.

3.5. Surface morphology studies

SEM images of selected samples are given in Fig. 8. According to surface morphology and crystal structure analyses of the coatings, plate-like and needle-like hydroxyapatite crystals were observed on the surface of the CoCrMo implants. This porous structure of the coating improves bonding ability and biocompatibility of the biometallic implants [9]. As seen in Fig. 8, run 3 has relatively poor hydroxyapatite crystal orientation compared with the others and did not exhibited a plate-like crystal formation. Relatively poor crystal formation of run 3 is consistent with the corrosion studies presented in Table 3 in a previous section. Surface morphologies of runs 6, 8, and 12 are better compared to run 3 and also in harmony with the more positive OCP, E_{corr}, high impedance and high R_p values. Runs 6, 8, and 12 are composed of dense packaged plate-like crystals. These dense hydroxyapatite layers are in good agreement with the observed high *in vitro* corrosion performance as predicted from the RSM model. The crystalline structure of run 16 (sample deposited at optimized parameters) has a dense plate-like hydroxyapatite crystal formation. *In vitro* corrosion performance of run 16 is also higher according to corrosion studies as expected by the RSM model.

3.6. FTIR analysis

FTIR spectroscopy result of a hydroxyapatite coating (optimized sample) is displayed in Fig. 9. A typical hydroxyapatite spectrum is

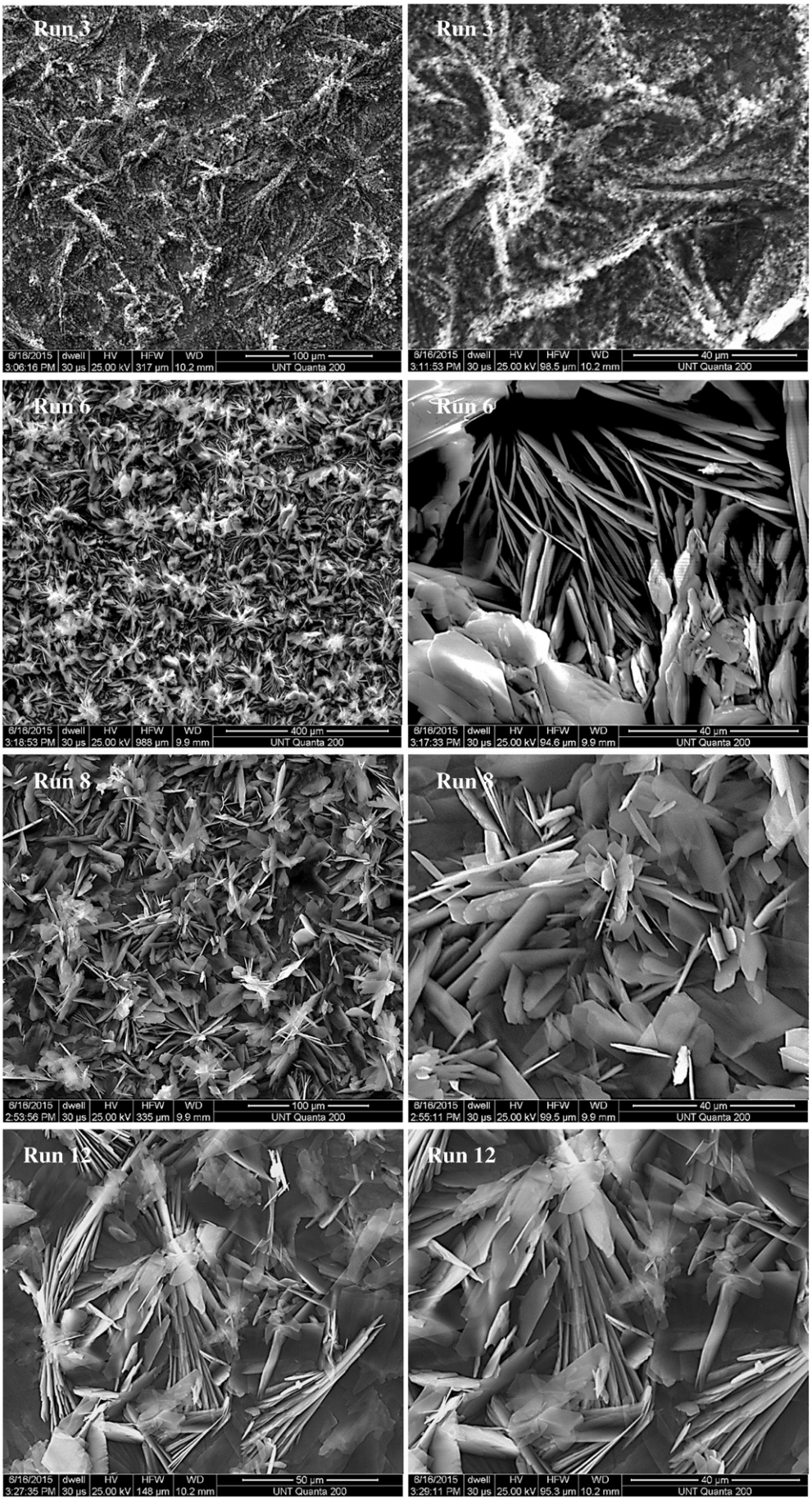
Run 3
8/16/2015 3:06:16 PM | dwell 30 µs | HV 25.00 kV | HFW 317 µm | WD 10.2 mm | 100 µm | UNT Quanta 200
Run 3
8/16/2015 3:11:53 PM | dwell 30 µs | HV 25.00 kV | HFW 98.5 µm | WD 10.2 mm | 40 µm | UNT Quanta 200
Run 6
8/16/2015 3:18:53 PM | dwell 30 µs | HV 25.00 kV | HFW 988 µm | WD 9.9 mm | 400 µm | UNT Quanta 200
Run 6
8/16/2015 3:17:33 PM | dwell 30 µs | HV 25.00 kV | HFW 94.6 µm | WD 9.9 mm | 40 µm | UNT Quanta 200
Run 8
8/16/2015 2:53:56 PM | dwell 30 µs | HV 25.00 kV | HFW 335 µm | WD 9.9 mm | 100 µm | UNT Quanta 200
Run 8
8/16/2015 2:55:11 PM | dwell 30 µs | HV 25.00 kV | HFW 99.5 µm | WD 9.9 mm | 40 µm | UNT Quanta 200
Run 12
8/16/2015 3:27:35 PM | dwell 30 µs | HV 25.00 kV | HFW 148 µm | WD 10.2 mm | 50 µm | UNT Quanta 200
Run 12
8/16/2015 3:29:11 PM | dwell 30 µs | HV 25.00 kV | HFW 95.3 µm | WD 10.2 mm | 40 µm | UNT Quanta 200

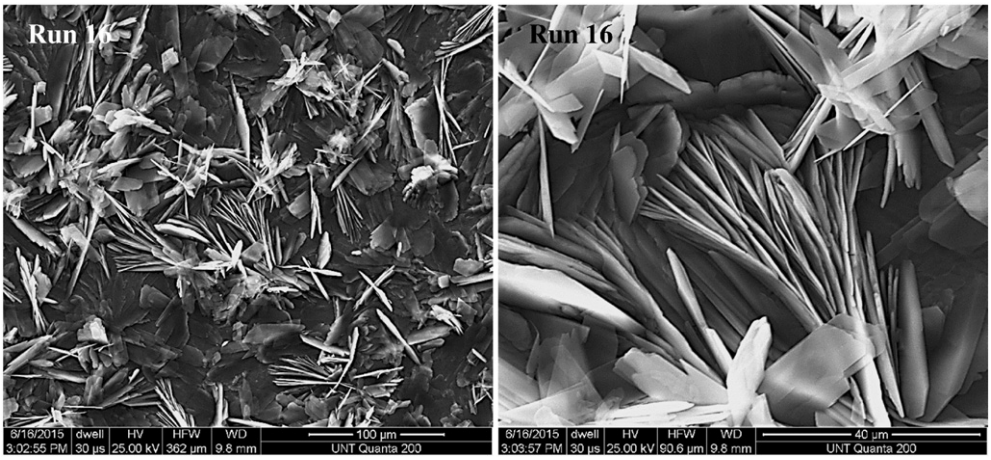

Fig. 8. SEM images of runs 3, 6, 8, 12 and 16.

observed which displays various vibrational modes for PO_4^{3-} and O–H groups. The strongest bands in all spectra are attributed to four possible vibrational modes in phosphate with strong bands between ~1000–1150 cm^{-1} and ~510–650 cm^{-1}, and two weaker bands at ~960 cm^{-1} and ~475 cm^{-1}. They correspond to asymmetrical stretching, symmetrical stretching, and bending vibrations for PO_4^{3-} [38]. The 475 cm^{-1} band corresponds to vibrational signals of the doubly degenerate O–P–O bending [39]. Two signals from triply degenerate O–P–O bending modes were observed at 560 and 600 cm^{-1} [39]. The band at 1010 cm^{-1} is the asymmetrical stretching vibrations of PO_4^{3-} [38]. The band around 1645 cm^{-1} corresponds to O–H bending vibrations in water [33]. A broad band associated with H_2O absorption is present in the range of 3000–3600 cm^{-1}. Observed peaks corresponding to run 16 (sample deposited at optimized parameters) are comparably sharp which indicates high crystallinity.

4. Conclusions

In this paper, electrodeposition of hydroxyapatite layers on metallic implants to improve biocompatibility and corrosion performance was investigated. Response Surface Methodology (RSM) and Central Composite Design (CCD) were successfully used in the optimization of step depositing parameters (initial potential, peak potential and scan rate) for electrodeposition of hydroxyapatite coatings. OCP, E_{corr}, and low frequency impedance values from electrochemical tests were used as responses for RSM models. The predicted and experimental results were in close agreement. While all models were successful and exhibited similar results, according to statistical analyses, the best fitting model was using the E_{corr} response model.

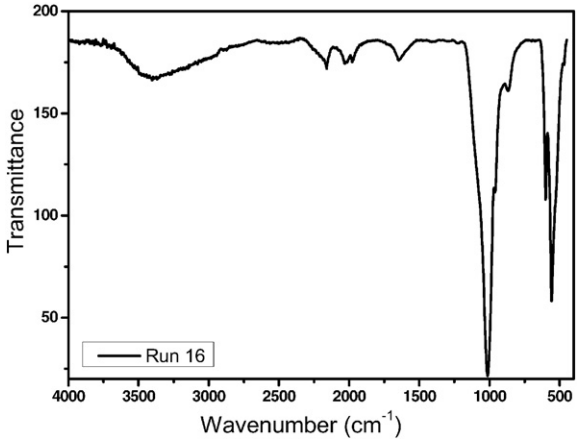

Fig. 9. FTIR spectra of run 16, sample deposited at optimized parameters.

Optimized step deposition parameters were found to be as an initial potential: −0.76 V, peak potential: −1.67 V and scan rate: 59.33 mV/s from the E_{corr} model. SEM analyses indicated that the surface of the sample fabricated at optimized parameters has a uniform, porous hydroxyapatite layer which improves biocompatibility of the implant. Characterization results and visible appearance of the samples indicated RSM and CCD methods were successful to optimize deposition conditions to fabricate hydroxyapatite coatings with high quality.

Results of this study conclude that computational methods such as RSM and CCD can be efficiently applied for the modeling and optimization of multiple deposition parameters. These optimized parameters can be used for modification surface of the CoCrMo implant devices to provide better *in vivo* performance.

Acknowledgments

The authors gratefully acknowledge the Center for Advanced Research and Technology (CART) at the University of North Texas for access to the SEM experimental facility used for this study. Mr. Coskun was supported by The Scientific and Technological Research Council of Turkey (TUBITAK).

References

[1] B. Park Joon, D. Bronzino Joseph, Biomaterials Principles and Applications, second ed. CRC Press, Florida, 2003.
[2] K. Grandfield, A. Palmquist, S. Gonçalves, A. Taylor, M. Taylor, L. Emanuelsson, P. Thomsen, H. Engqvist, Free form fabricated features on CoCr implants with and without hydroxyapatite coating in vivo: a comparative study of bone contact and bone growth induction, J. Mater. Sci. Mater. Med. 22 (2011) 899–906.
[3] P.H. Long, Medical devices in orthopedic applications, Toxicol. Pathol. 36 (2008) 85–91.
[4] J.C. Escobedo, J.C. Ortiz, J.M. Almanza, D.A. Cortes, Hydroxyapatite coating on a cobalt base alloy by investment casting, Scr. Mater. 54 (2006) 1611–1615.
[5] M. Grecu, G. Novac, D. Ionita, C. Ungureanu, Incorporation of tobramycin biomimetic in hydroxyapatite coating on CoCrMo alloy and its antimicrobial activity, Rev. Chim. (Bucharest, Rom.) 62 (2011) 352–356.
[6] W.Q. Yu, J. Qui, F.Q. Zhang, In vitro corrosion study of different TiO_2 nanotube layers on titanium in solution with serum proteins, Colloids Surf. B 84 (2011) 400–405.
[7] L.N. Wang, J.J. Luo, Preparation of hydroxyapatite coating on CoCrMo implant using an effective electrochemically-assisted deposition pretreatment, Mater. Charact. 62 (2011) 1076–1086.
[8] Z. Sam, Hydroxyapatite Coatings for Biomedical Applications, CRC Press, Boca Raton, FL, 2013.
[9] Q. Zhang, Y. Lenga, R. Xin, A comparative study of electrochemical deposition and biomimetic deposition of calcium phosphate on porous titanium, Biomaterials 26 (2005) 2857–2865.
[10] M.A. Lopez-Heredia, P. Weiss, P. Layrolle, An electrodeposition method of calcium phosphate coatings on titanium alloy, J. Mater. Sci. Mater. Med. 18 (2007) 381–390.

[11] R. Drevet, O. Aaboubi, H. Benhayoune, In vitro corrosion behavior of electrodeposited calcium phosphate coatings on Ti6Al4V substrates, J. Solid State Electrochem. 16 (2012) 3069–3077.
[12] M.B. Kannan, Enhancing the performance of calcium phosphate coating on a magnesium alloy for bioimplant applications, Mater. Lett. 76 (2012) 109–112.
[13] H. Wang, N. Eliaz, L.W. Hobbs, The nanostructure of an electrochemically deposited hydroxyapatite coating, Mater. Lett. 65 (2011) 2455–2457.
[14] Q. Yuan, T.D. Golden, Electrochemical study of hydroxyapatite coatings on stainless steel substrates, Thin Solid Films 518 (2009) 55–60.
[15] D. Gopi, J. Indira, L. Kavitha, A comparative study on the direct and pulsed current electrodeposition of hydroxyapatite coatings on surgical grade stainless steel, Surf. Coat. Technol. 206 (2012) 2859–2869.
[16] A. Kar, K.S. Raja, M. Misra, Electrodeposition of hydroxyapatite onto nanotubular TiO_2 for implant applications, Surf. Coat. Technol. 201 (2006) 3723–3731.
[17] D.Y. Lin, X.X. Wang, Electrodeposition of hydroxyapatite coating on CoNiCrMo substrate in dilute solution, Surf. Coat. Technol. 204 (2010) 3205–3213.
[18] V. DeLeon, T.D. Golden, Effect of electrochemical parameters on the morphology and Ca/P ratio of deposited apatite coatings on metal and alloy substrates, ECS Trans. 33 (2011) 43–50.
[19] R.G. Brereton, Chemometrics: Data Analysis for the Laboratory and Chemical Plant, Wiley, Chichester, 2003.
[20] E. Yücel, N. Güler, Y. Yücel, Optimization of deposition conditions of CdS thin films using response surface methodology, J. Alloys Compd. 589 (2014) 207–212.
[21] E. Yücel, Y. Yücel, Optimization of zinc sulfide thin film coating process using response surface methodology, J. Mater. Sci. Mater. Electron. 26 (2015) 196–203.
[22] E. Yücel, Y. Yücel, İ. Belenli, Optimization of fabrication conditions of MgB_2/Fe superconducting tapes using response surface methodology, J. Mater. Sci. Mater. Electron. 23 (2012) 1284–1292.
[23] E. Yücel, Y. Yücel, B. Beleli, Optimization of synthesis conditions of PbS thin films grown by chemical bath deposition using response surface methodology, J. Alloys Compd. 642 (2015) 63–69.
[24] E. Yücel, Y. Yücel, D. Gökhan, Computer assisted optimization of copper sulphide thin film coating parameters on glass substrates, Appl. Surf. Sci. 351 (2015) 904–910.
[25] E. Yücel, Y. Yücel, B. Beleli, Process optimization of deposition conditions of PbS thin films grown by successive ionic layer adsorption and reaction (SILAR) method using response surface methodology, J. Cryst. Growth 422 (2015) 1–7.
[26] M.İ. Coşkun, İ.H. Karahan, Y. Yücel, Optimized electrodeposition concentrations for hydroxyapatite coatings on CoCrMo biomedical alloys by computational techniques, Electrochim. Acta 150 (2014) 46–54.
[27] J. Wang, Y. Chao, Q. Wan, Z. Zhu, H. Yu, Fluoridated hydroxyapatite coatings on titanium obtained by electrochemical deposition, Acta Biomater. 5 (2009) 1798–1807.
[28] M. Shirkhanzadeh, Direct formation of nanophase hydroxyapatite on cathodically polarized electrodes, J. Mater. Sci. Mater. Med 9 (1998) 67–72.
[29] M.İ. Coşkun, İ.H. Karahan, T.D. Golden, Computer assisted corrosion analysis of hydroxyapatite coated CoCrMo biomedical alloys, Surf. Coat. Technol. 275 (2015) e1–e9.
[30] R. Drevet, A. Lemelle, V. Untereiner, M. Manfait, G.D. Sockalingum, H. Benhayoune, Morphological modifications of electrodeposited calcium phosphate coatings under amino acids effect, Appl. Surf. Sci. 268 (2013) 343–348.
[31] N. Eliaz, M. Eliyahu, Electrochemical processes of nucleation and growth of hydroxyapatite on titanium supported by real-time electrochemical atomic force microscopy, J. Biomed. Mater. Res. Part A 80 (3) (2007) 621–634.
[32] D. Gopi, S. Ramya, D. Rajeswari, L. Kavitha, Corrosion protection performance of porous strontium hydroxyapatite coating on polypyrrole coated 316L stainless steel, Colloids Surf. B 107 (2013) 130–136.
[33] M. Jamesh, S. Kumar, T.S.N.S. Narayanan, Electrodeposition of hydroxyapatite coating on magnesium for biomedical applications, J. Coat. Technol. Res. 9 (4) (2012) 495–502.
[34] A. Kazek-Kęsik, M. Krok-Borkowicz, E. Pamuła, W. Simka, Electrochemical and biological characterization of coatings formed on Ti–15Mo alloy by plasma electrolytic oxidation, Mater. Sci. Eng. C 43 (2014) 172–181.
[35] X. Zhang, Q. Li, L. Li, P. Zhang, Z. Wang, F. Chen, Fabrication of hydroxyapatite/stearic acid composite coating and corrosion behavior of coated magnesium alloy, Mater. Lett. 88 (2012) 76–78.
[36] N. Eliaz, T.M. Sridhar, U.K. Mudali, B. Raj, Electrochemical and electrophoretic deposition of hydroxyapatite for orthopaedic applications, Surf. Eng. 21 (2005) 238–242.
[37] Y.W. Song, D.Y. Shan, E.H. Han, Electrodeposition of hydroxyapatite coating on AZ91D magnesium alloy for biomaterial application, Mater. Lett. 62 (2008) 3276–3279.
[38] D. Qiu, L. Yang, Y. Yin, A. Wang, Preparation and characterization of hydroxyapatite/titania composite coating on NiTi alloy by electrochemical deposition, Surf. Coat. Technol. 205 (2011) 3280–3284.
[39] W.H. Lee, C.Y. Loo, A.V. Zavgorodniy, R. Rohanizadeh, High protein adsorptive capacity of amino acid-functionalized hydroxyapatite, J. Biomed. Mater. Res. Part A 101 (2013) 873–883.